Received: 25 June 2016 | Accepted: 22 September 2016

DOI: 10.1111/jace.14601

ORIGINAL ARTICLE

Journal of the American Ceramic Society

New eight-layer twinned hexagonal perovskite microwave dielectric ceramic $Ba_8NiNb_6O_{24}$

Fengqiong Tao[1] | Xiaoming Wang[2] | Mielu Gong[1] | Fengqi Lu[1] | Mathieu Allix[3] | Xiaojun Kuang[1] | Liang Fang[1]

[1]Guangxi Ministry-Province Jointly Constructed Cultivation Base for State Key Laboratory of Processing for Nonferrous Metal and Featured Materials, Guangxi Universities Key Laboratory of Non-ferrous Metal Oxide Electronic Functional Materials and Devices, College of Materials Science and Engineering, Guilin University of Technology, Guilin, China

[2]Beijing National Laboratory for Molecular Sciences, The State Key Laboratory of Rare Earth Materials Chemistry and Applications, College of Chemistry and Molecular Engineering, Peking University, Beijing, China

[3]CNRS, CEMHTI UPR3079, University of Orléans, Orléans, France

Correspondence
Xiaojun Kuang and Liang Fang, Guangxi Ministry-Province Jointly Constructed Cultivation Base for State Key Laboratory of Processing for Nonferrous Metal and Featured Materials Guangxi Universities Key Laboratory of Non-ferrous Metal Oxide Electronic Functional Materials and Devices College of Materials Science and Engineering Guilin University of Technology Guilin China.
Email: kuangxj@glut.edu.cn and fanglianggl001@yahoo.cn

Funding information
U.S. Department of Energy, Office of Science, Office of Basic Energy Sciences, Grant/Award Number: DE-AC02-06CH11357.

Abstract

A new eight-layer hexagonal perovskite $Ba_8NiNb_6O_{24}$ was synthesized via the high-temperature solid-state reaction and its structure was characterized using selected area electron diffraction, high-resolution transmission electron microscopy, and synchrotron X-ray diffraction. Unlike the eight-layer ordered shifted $Ba_8CoNb_6O_{24}$ and $Ba_8ZnNb_6O_{24}$, $Ba_8NiNb_6O_{24}$ adopts a twinned structure with stacking sequence $(ccch)_2$ for the BaO_3 layers and displays more disordered cation and vacancies over the face-sharing octahedral (FSO) sites than the twinned tantalates $Ba_8MTa_6O_{24}$ (M=Zn, Ni, Co). The stabilization of twinned structure and cation/vacancy ordering in $Ba_8NiNb_6O_{24}$ composition is correlated with the smaller size difference between Ni^{2+} and Nb^{5+} in comparison with those between $(Zn/Co)^{2+}$ and Nb^{5+} in the shifted $Ba_8CoNb_6O_{24}$ and $Ba_8ZnNb_6O_{24}$. The $Ba_8NiNb_6O_{24}$ pellet exhibits high dielectric permittivity $\varepsilon_r \sim 40$, modest $Qf \sim 41\,319$ GHz, and large temperature coefficient of resonant frequency $\tau_f \sim 60$ ppm/°C. The lower Qf value compared with the high-Q $Ba_8MTa_6O_{24}$ is ascribed to the reduced short-range B-cationic ordering inside the FSO dimers in $Ba_8NiNb_6O_{24}$. These results contribute to understanding the interplay among chemical composition, structure, and dielectric properties of the eight-layer twinned and shifted hexagonal perovskites.

KEYWORDS
cation ordering, eight-layer hexagonal perovskite, microwave dielectric property, twin-shift option

1 | INTRODUCTION

High-performance dielectric materials (permittivity ε_r within 20-50, Qf>30 000 GHz, where Q is equal to inverse dielectric loss tan δ and f is resonant frequency, and temperature coefficient of resonant frequency, $\tau_f \sim \pm 3$ ppm/°) are required as resonator and filter components for the base station of mobile phone networks.[1] Considerable attention has been focused on complex perovskites of tantalates and niobates due to their excellent

microwave dielectric performance.[1-4] For example, 2:1-ordered $Ba_3MTa_2O_9$ (M=Zn, Mg) resonators possess modest $\varepsilon_r \sim 30$, near-zero τ_f, and superior quality factors $Qf \sim 90\,000$-$160\,000$ GHz, offering efficient utilization of the allocated electromagnetic frequency window.[1,4] However, these complex perovskite resonators suffer from the requirement of prolonged high-temperature annealing to control the cationic ordering in order to achieve high-quality factors.[1,4-6]

In the past two decades, there has been growing interest in developing hexagonal perovskites as dielectric resonators and filters.[7-13] Hexagonal perovskite oxides contain the same building units of close-packed AO_3 layers found in cubic perovskites, but arranged with pure hexagonal or mixed cubic-hexagonal close packing. According to different alternate cubic (c) and hexagonal (h) sequences, hexagonal perovskites are classified into two major types of twinned or shifted structures depending on whether a single hexagonal layer or two consecutive hexagonal layers separate the cubic blocks,[14] respectively. Among the various hexagonal perovskite dielectrics, eight-layer B-site-deficient hexagonal perovskites are the most fascinating compounds owing to (i) their high Qf values comparable to the values of complex tantalate perovskites compositions and (ii) the interesting twin-shift phase competition and cationic ordering. $Ba_8MTa_6O_{24}$ (M=Zn, Ni, Co)[11,12,15,16] adopts a eight-layer twinned structure with a $(ccch)_2$ stacking sequence for BaO_3 layers and the B-site vacancies and M^{2+} cations are distributed in a partially ordered manner within the face-sharing octahedral (FSO) dimers. These materials exhibit $\varepsilon \sim 29$, high Qf values ~70 000-90 000 GHz, although the relatively high τ_f values within ~30-45 ppm/°C.[11,12,15,16] The search for cheaper niobate counterparts of the $Ba_8MTa_6O_{24}$ led to the discovery of the eight-layer shifted $Ba_8CoNb_6O_{24}$[13] and $Ba_8ZnNb_6O_{24}$[17] compounds. These two shifted niobates show larger $\varepsilon_r \sim 31$-35, but lower Qf values ~35 000-50 000 GHz than the twinned tantalates, and positive τ_f values within ~16-44 ppm/°C similar to the twinned tantalates. The shifted structure adopts a *ccccccchh* stacking sequence for BaO_3 layers and vacancy ordering occurs between two consecutive hexagonal (h) layers, resulting in a completely vacant octahedral layer located at the middle of the FSO trimers. These empty octahedral layers isolate the perovskite blocks consisting of seven consecutive corner-sharing octahedral (CSO) layers, where Co/Zn cations are confined in the central octahedral sites of the CSO blocks, leading to single Co/Zn layers apart from each other by ~1.9 nm. The out of center displacement toward empty octahedral layers for the highly charged d^0 Nb^{5+} next to the empty octahedral layers owing to the second-order Jahn-Teller (SOJT) effect is necessary to stabilize the oxide anions in the empty octahedral layers, thus contributing to the unusual nanometer scale B-cation ordering in $Ba_8CoNb_6O_{24}$[13] and $Ba_8ZnNb_6O_{24}$.[17]

The stabilization of the twin-shift configuration for the eight-layered tantalate and niobate hexagonal perovskites described above has been associated with the subtle difference between SOJT effects of Ta^{5+} and Nb^{5+}. The Ta^{5+}-O^{2-} bonding is more ionic than Nb^{5+}-O^{2-}[4,17]; thus compared with Nb^{5+}, the out of center distortion in the oxygen octahedron of Ta^{5+} is not sufficient for stabilizing oxide anions in the empty octahedral layer and therefore destabilizing the shifted structure.[17] Forming a twinned structure with shorter periodicity for the B-site vacancy and B-cations is more energy favorable for the tantalate compositions.

In order to deeply understand the fundamental chemistry on the structural behaviors of the eight-layer hexagonal perovskites and correlate their dielectric performance with the chemical compositions and structures, we exploit more analogues within the eight-layer hexagonal perovskite families. So far there is no attention on the phase formation and dielectric properties for the niobate counterpart of the twinned $Ba_8NiTa_6O_{24}$. In this study, we present the stabilization of eight-layer twinned hexagonal perovskite for the $Ba_8NiNb_6O_{24}$ composition and the microwave dielectric properties of the $Ba_8NiNb_6O_{24}$ ceramic. The twinned-phase stability of $Ba_8NiNb_6O_{24}$ is correlated with B-cationic size difference, which controls the cation/vacancy ordering therefore impacts the dielectric performance of $Ba_8NiNb_6O_{24}$.

2 | EXPERIMENTAL PROCEDURE

The $Ba_8NiNb_6O_{24}$ samples were prepared by high-temperature solid-state reaction using $BaCO_3$ (99%, Aladdin, Shanghai, China), NiO (99.5%, Aladdin), and Nb_2O_5 (99.99%, Aladdin) powders as starting materials. These starting materials were weighed according to the correct stoichiometry and mixed in ethanol with an agate mortar and pestle. The dried mixtures were calcined at 1200°C for 12 hour in alumina crucibles. These calcined powders were then ground, pressed into pellets under a pressure of 330 MPa, and fired at 1300-1500°C for 12 hour on platinum foil with heating and cooling rates of 5°C/min. The resulting pellets were ground into fine powder for phase-formation examination and structure investigation using X-ray powder diffraction (X'PertPRO diffractometer, Almelo, the Netherlands).

The pellets of $Ba_8NiNb_6O_{24}$ for electrical property measurements were prepared via the following processing. Stoichiometric raw materials of $BaCO_3$, NiO, and Nb_2O_5 in ~6 g batches were weighed and mixed in ethanol with an agate and pestle. The powders were precalcined at 1200°C

for 12 hour, mixed with a 5% polyvinyl alcohol solution as an organic binder, and then pressed into pellets with a cold-isostatic pressing facility under a pressure of ~250 MPa. The pellets were sintered at 1500°C for 4 hour on platinum foil with heating and cooling rates of 5°C/min, leading to 95% of the theoretical X-ray density. The densities of the pellets were calculated using the geometric sizes (diameters and thicknesses) and the masses of the pellets.

The phase assemblages were examined by laboratory X-ray powder diffraction which was performed on a Panalytical X'PertPRO diffractometer with Cu$K\alpha$ radiation and equipped with an Anton Parr HTK 1200N high-temperature attachment. Variable-temperature X-ray diffraction (VT-XRD) data collection was carried out from room temperature up to 1100°C at a temperature step of 25°C with an equilibration time of ~5 minute before data collection (for ~8 minute at each temperature set point). High-intensity and high-resolution synchrotron powder diffraction (SPD) data were collected on the 11BM diffractometer at the Advanced Photo Source (Argonne National Laboratory, USA). The powder was loaded in a 0.3-mm diameter glass capillary, and data were collected at room temperature over the 0.5-50° 2θ range using a step size of 0.001° and wavelength of λ=0.459300 Å. Rietveld analysis was carried out using the Topas Academic.[18] Bond valence sums (BVSs) were calculated by Brown and Altermatt's method.[19] The selected area electron diffraction (SAED) and high-resolution transmission electron microscopy (HRTEM) experiments were performed on a JOEL JEM-2100F (Tokyo, Japan) transmission electron microscope operating at 200 kV (point resolution of 1.9 Å).

The surface microstructures of the pellets were examined using a Hitachi (Tokyo, Japan) S4800 scanning electron microscopy (SEM). Before the SEM measurement, gold was sprayed on the surface to form a thin conducting layer. Energy dispersive X-ray spectroscopy (EDS) elementary analysis was carried out during the SEM experiment. The microwave dielectric properties were measured by the Hakki-Coleman dielectric resonator method[20] with the TE_{011} mode using an Agilent N5230A network analyzer (Palo Alto, CA). The temperature coefficient of resonate frequency τ_f values were measured from 25°C to 85°C. AC impedance spectroscopy (IS) measurements in air were performed at room temperature to 800°C using a Solartron 1260A impedance/gain-phase analyzer (Farnborough, UK) over the frequency range from 10^{-1} to 10^7 Hz. Before the IS measurement, the pellet was coated with platinum paste and fired at 800°C for 40 minute in order to remove the organic components to form electrodes. The complex impedance data were analyzed with the ZView software. Ultraviolet and visible (UV-Vis) light absorption spectra were obtained via measurements of diffuse reflectance on the dry-pressed disk samples using a UV3600 UV-Vis spectrometer fitted with $BaSO_4$ as standard material in the 200-1200 nm wavelength region with a resolution of 0.1 nm.

3 | RESULTS AND DISCUSSION

3.1 | Structure

Figure 1 shows XRD data of $Ba_8NiNb_6O_{24}$ samples fired at various temperatures within 1200°C-1500°C for 12 hour. In 1200°C-1300°C, the $Ba_8NiNb_6O_{24}$ composition formed mixtures containing cubic $Ba_3NiNb_2O_9$ (three-layered perovskite structure, referred to as 3C) and hexagonal $Ba_5Nb_4O_{15}$ (five-layered hexagonal perovskite structure, referred to as 5H) as major phases as well as a minor monoclinic $Ba_4Nb_2O_9$ phase. An eight-layer hexagonal phase (referred to as 8H) appeared at 1400°C as a minor phase and the 3C and 5H phases disappeared at 1500°C, resulting in single 8H phase eventually. The EDS elementary analysis of this 8H-phase gave an average cationic composition of $Ba_8Ni_{0.86(1)}Nb_{6.7(4)}$, close to the expected composition. The indexation led to hexagonal cell parameters corresponding to an 8H-phase ($a \sim 10.073$ Å, $c \sim 18.992$ Å), similar to $Ba_8MTa_6O_{24}$.[11,12,15,16] The SAED experiments (Figure 2A) further confirmed this unit cell and revealed reflection conditions of 00l: l=2n and $hh\bar{l}$: l=2n, leading to three possible space groups: $P6_3cm$, $P\bar{6}c2$, and $P6_3/mcm$. The HRTEM image (Figure 2B) recorded along [010] indicates a twinned structure with a stacking sequence $(hccc)_2$ for the closed packed BaO_3 layers in $Ba_8NiNb_6O_{24}$. VT-XRD data were collected from 25°C to 1100°C in air, which shows that the eight-layer phase is stable with linear thermal expansion over the measured temperature region (Figure 3), giving the coefficient of thermal expansion for

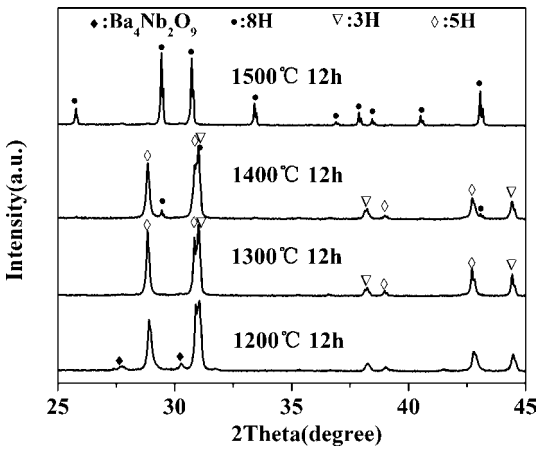

FIGURE 1 X-ray diffraction patterns of $Ba_8NiNb_6O_{24}$ samples fired at different temperature. 8H, 5H, and 3C denote eight-layer hexagonal $Ba_8NiNb_6O_{24}$, five-layer hexagonal $Ba_5Nb_4O_{15}$, and three-layer cubic $Ba_3NiNb_2O_9$ phases, respectively

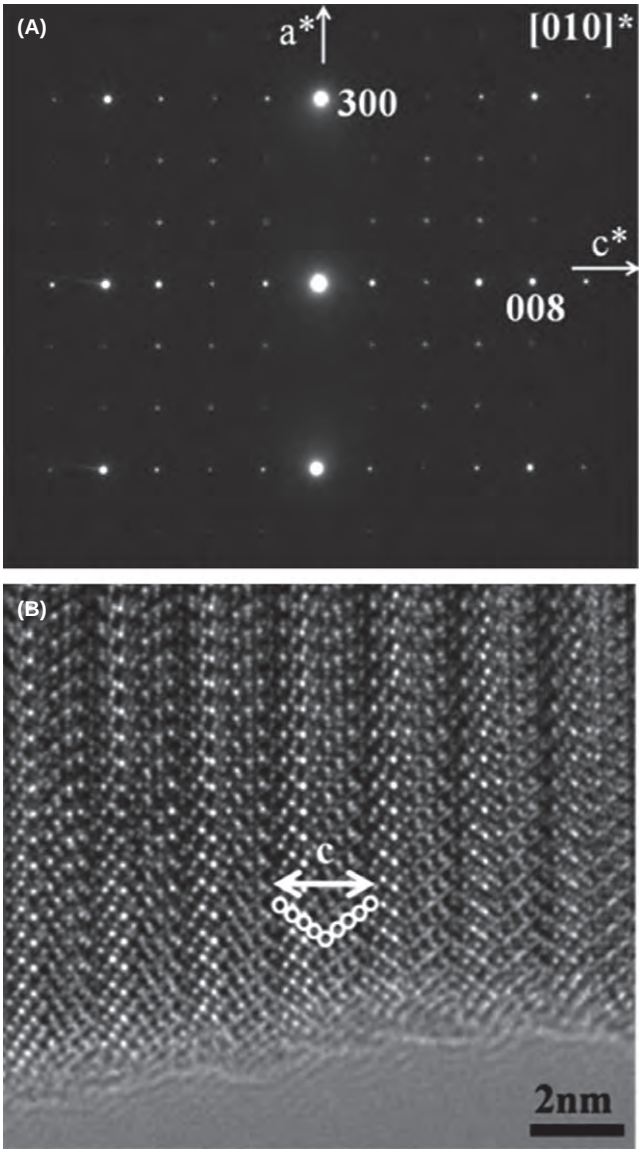

FIGURE 2 (A) Selected area electron-diffraction pattern projection along the [010] direction and (B) high-resolution transmission electron microscopy image for $Ba_8NiNb_6O_{24}$ recorded along the same direction. The twinned stacking feature is highlighted by the empty white circles in (B). The a* and c* in (A) denote the reciprocal a and c axes

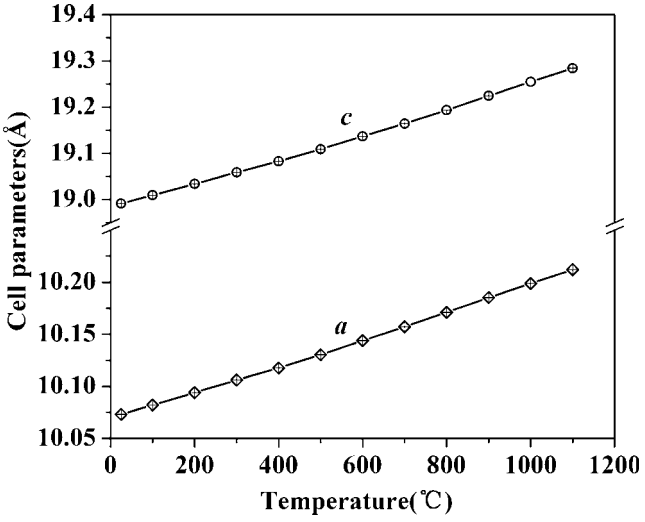

FIGURE 3 Temperature dependency of cell parameters for $Ba_8NiNb_6O_{24}$

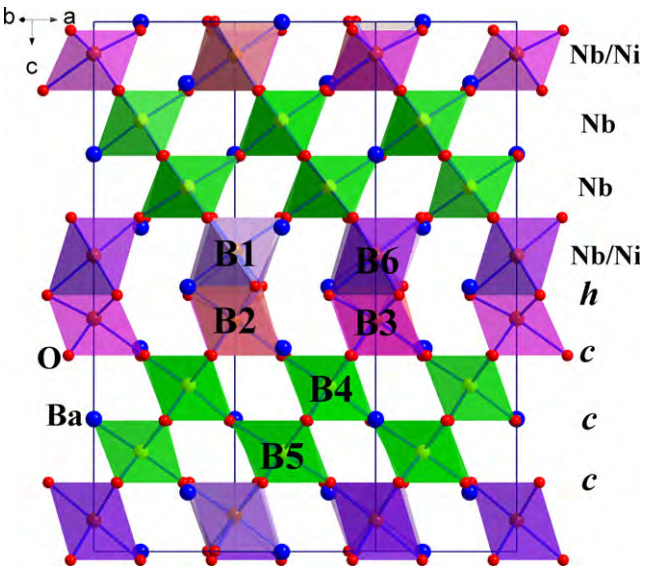

FIGURE 4 Structural model of the eight-layer twinned hexagonal perovskite $Ba_8NiNb_6O_{24}$. The B4 and B5 corner-sharing octahedral sites (in green) stand for 100% Nb, the face-sharing octahedral dimers B1–B2 and B3–B6 contain Nb, Ni plus vacancies. The blue and red spheres denote the Ba and O atoms, respectively [Color figure can be viewed at wileyonlinelibrary.com]

the volume as ~40.4 ppm/°C. However, the prolonged firing at 1400°C-1500°C for 24 hour led to partial decomposition, as suggested by the extra reflection from $Ba_5Nb_4O_{15}$.

Rietveld analysis of the $Ba_8NiNb_6O_{24}$ structure was performed on SPD data using as a starting point the $Ba_8NiTa_6O_{24}$ structural model[21] in the acentric space group $P6_3cm$, which contains three FSO (B1-B3) and two CSO (B4-B5) B-sites (Figure 4). The refinement led to reliability factors R_{wp} ~ 11.57%, and R_p ~ 8.68%, essentially confirming the twinned structure for $Ba_8NiNb_6O_{24}$. The site occupancies were then refined over all of the five B-sites, which confirmed that the CSO B-sites are fully occupied by Nb and the preference of Ni atoms in the FSO B2 site over the FSO B1 and B3 sites, similar to $Ba_8NiTa_6O_{24}$.[21] However, the B3 site in $Ba_8NiNb_6O_{24}$ appears partially occupied by ~80% Nb, unlike $Ba_8NiTa_6O_{24}$ where B3 site are fully occupied by Ta and the neighboring B-sites in the FSO dimers are empty.[21] This implies that the B-cations in $Ba_8NiNb_6O_{24}$ could be more disordered than those in the tantalate analogues. Difference Fourier map was calculated and the plot at z=0.44 slice (Figure 5) reveals apparent

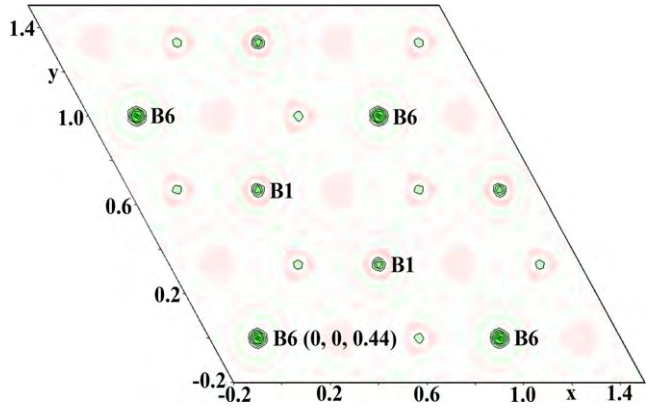

FIGURE 5 Calculated difference Fourier map at z=0.44 slice for $Ba_8NiNb_6O_{24}$ [Color figure can be viewed at wileyonlinelibrary.com]

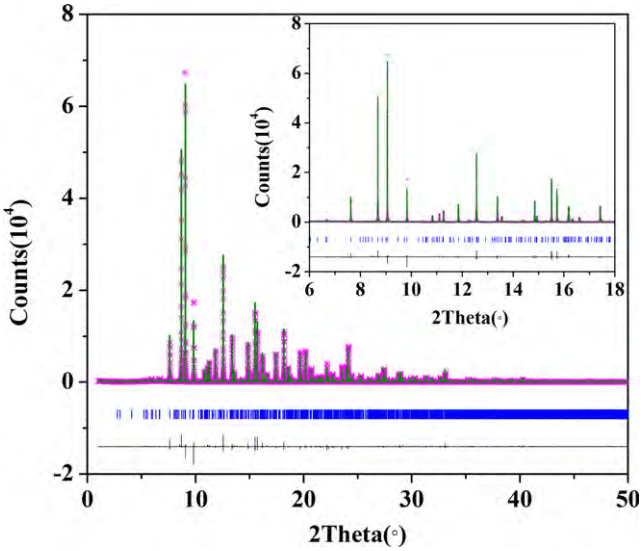

FIGURE 6 Rietveld plot of the synchrotron powder diffraction data for $Ba_8NiNb_6O_{24}$. The inset enlarges the fit within the 8°-18° 2θ range. The reliability factors are: R_{wp} ~ 10.74%, R_p ~ 8.55%, and R_B ~ 3.07% [Color figure can be viewed at wileyonlinelibrary.com]

positive scatting density around a 2*a* site (0, 0, 0.44), which is at the level of B1 site and forms a FSO dimer with B3 site. This confirms that the FSO cations are more disordered in $Ba_8NiNb_6O_{24}$ than $Ba_8NiTa_6O_{24}$, where this 2*a* site is empty. Therefore, this new 2*a* site (labeled as B6 in Figure 4) was added into the structure of $Ba_8NiNb_6O_{24}$ for subsequent refinements. However, refinement of the occupancies of Ni^{2+} and Nb^{5+} plus vacancies over the four FSO B-sites (i.e., B1-B2 and B3-B6 dimers) remains challenging. Thus, the occupancies of Ni^{2+} and Nb^{5+} on all the FSO sites were refined by a simulated annealing approach subject to a chemical constrain according to the nominal composition. Such method has been proved reliable and successful on determining different complex structures from powder diffraction data.[7,22-24] The refinement converged to R_{wp} ~ 10.74% and R_p ~ 8.55% and led to 0.60 (9) Nb/0.40(9) □ (□ denotes vacancy) on the B1 site and 0.25(2)Nb/0.75(2) Ni on the B2 site for the FSO B1-B2 dimers, 0.8(2) Nb/0.2(2) (on the B3 site) and 0.5(1) Nb/0.5 (2)□ on the B6 site for the FSO B3-B6 dimers. Therefore, the refinement confirms the short-range ordering inside the FSO dimers in $Ba_8NiNb_6O_{24}$, which excludes the $P\bar{6}c2$ space group for $Ba_8NiNb_6O_{24}$ because the FSO sites within the same FSO dimer in the structural model in $P\bar{6}c2$ are equivalent, similarly to $Ba_8MTa_6O_{24}$ (*M*=Ni and Zn)[11,21] and $Ba_8Ga_{4-x}Ta_{4+0.6x}O_{24}$[7] cases. Rietveld plot of the SPD data is shown in Figure 6 and the final refined structural parameters and bond lengths of $Ba_8NiNb_6O_{24}$ are listed in Tables 1 and 2, respectively.

The inaccessibility of shifted phase on $Ba_8NiNb_6O_{24}$ composition implies that both M^{2+} and Nb^{5+} cations have cooperative interaction for stabilizing the shifted phase in $Ba_8MNb_6O_{24}$. In the ordered shifted $Ba_8ZnNb_6O_{24}$ and $Ba_8CoNb_6O_{24}$ phases, Zn^{2+} and Co^{2+} (in high-spin configuration) cations have large ionic radii 0.74-0.745 Å and the big size-contrast between $(Zn/Co)^{2+}$ and Nb^{5+}(0.64 Å) also plays important role on the nanometer-scale cation ordering, which could be parallel to the SOJT distortion of Nb^{5+} required for stabilizing the oxide anions in the empty octahedral layers. While Ni^{2+} has a smaller size (0.69 Å) than Zn^{2+} and Co^{2+}, the size difference between Ni^{2+} and Nb^{5+} might be not large enough to drive nanometer scale cation ordering, thus destabilizing the shifted phase. Although formation of the twinned structure results in FSO cationic repulsion, the twinned structure has a shorter periodicity of vacancies and the smaller Ni^{2+} is more favorable for the FSO M^{2+}-Nb^{5+} dimers in the twinned structure compared with Zn^{2+} and Co^{2+}. Both the shorter periodicity of vacancies and the smaller Ni^{2+} ions could contribute to the stabilization of the twinned structure for the $Ba_8NiNb_6O_{24}$ composition. The smaller difference between the ionic radius of Ni^{2+} and Nb^{5+} may also contribute to more disordered FSO B-sites in the twinned $Ba_8NiNb_6O_{24}$, in comparison with the twinned $Ba_8MTa_6O_{24}$ tantalates.[11,21] The cationic ordering in $Ba_8NiNb_6O_{24}$ is similar to another eight-layer twinned analogue, $Ba_8Ga_{4-x}Ta_{4+0.6x}O_{24}$,[7] in which the close sizes of Ta^{5+} (0.64 Å) and Ga^{3+} (0.62 Å) also lead to less ordered cationic distribution compared with $Ba_8MTa_6O_{24}$. It should be noted here that although the size difference between Ni^{2+} and Ta^{5+} in $Ba_8NiTa_6O_{24}$ is identical to that between Ni^{2+} and Nb^{5+} in $Ba_8NiNb_6O_{24}$, the former displays more ordered B-cationic distribution than the latter.[21] This indicates that $Ba_8NiNb_6O_{24}$ has potential to display more ordered B-cationic distribution. Given the B-cationic ordering in the complex perovskite niobates is usually more sluggish than the tantalates counterparts,[3,25] the short-range cationic ordering could be kinetically controlled in

TABLE 1 Final refined structural parameters for $Ba_8NbNi_6O_{24}$[a]

Atom	Site	*x*	*y*	*z*	Occupancy	B_{iso}(Å^2)	BVS
Ba_1	2*a*	0	0	1/4	1	0.89(7)	2.50
Ba_2	4*b*	1/3	2/3	0.2519(3)	1	0.99(4)	2.28
Ba_3	6*c*	0.6725(2)	0	0.6162(3)	1	1.10(4)	2.41
Ba_4	6*c*	0.3335(3)	0	0.8882(3)	1	1.14(4)	2.30
Ba_5	6*c*	0.3330(3)	0	0.5007(3)	1	0.75(1)	2.15
Nb_1	4*b*	1/3	2/3	0.4311(3)	0.60(9)	0.77(7)	3.12
Nb_2	4*b*	1/3	2/3	0.0629(3)	0.25(2)	0.46(8)	3.67
Ni_2	4*b*	1/3	2/3	0.0629(3)	0.75(2)	0.46(8)	1.83
Nb_3	2*a*	0	0	0.0604(4)	0.8(2)	0.8(1)	4.68
Nb_4	6*c*	0.3347(3)	0	0.6867(3)	1	0.34(5)	4.89
Nb_5	6*c*	0.6680(3)	0	0.8127(3)	1	0.35(4)	4.73
Nb_6	2*a*	0	0	0.4416(5)	0.5(1)	0.2(2)	3.15
O_1	6*c*	0.519(1)	0	0.2530(9)	1	0.1(3)	1.99
O_2	6*c*	0.161(2)	0.161(2)	0.870(1)	1	0.9(5)	1.74
O_3	6*c*	0.165(2)	0.165(2)	0.5162(7)	1	0.4(3)	2.23
O_4	12*d*	0.650(1)	0.158(1)	0.4992(9)	1	0.9(1)	1.70
O_5	12*d*	0.3303(9)	0.1697(9)	0.2528(8)	1	0.5(2)	1.94
O_6	12*d*	0.666(2)	0.167(2)	0.1303(8)	1	0.7(3)	1.87
O_7	6*c*	0.180(2)	0.180(2)	0.130(1)	1	1.1(5)	2.15
O_8	12*d*	0.480(1)	0.324(2)	0.8700(7)	1	0.5(3)	2.13

[a]a=10.07340(1) Å, c=18.99157(2) Å, V=1668.953(4) Å^3, space group: $P6_3cm$, Z=3. The bond valence sums (BVSs) for the oxygen sites were calculated with the mixed and partial occupancies of the B-sites taken into consideration. The "b" and "d" symbols are Wyckoff letters for the crystallographic sites.

$Ba_8NiNb_6O_{24}$. Rietveld refinements of the XRD data of the annealed sample at 1400°C-1500°C for 12-24 hour were performed, which did not show apparent B-site cationic ordering enhancement.

Aside from the cationic size, the d-shell electronic configuration of the transitional metal cation M^{2+} has a strong link with the chemical bonding with oxide anions in the FSO dimers. Therefore, the latter could affect the twin-shift option in the eight-layer hexagonal perovskites. The complete elucidation of how the electronic configuration affects the twin-shift competition in eight-layer hexagonal perovskites could require consideration of the electronic structure from density-functional theory calculation and awaits full exploration of new eight-layer phases in wider compositional range.

3.2 | Electrical properties

The surface morphology of dense $Ba_8NiNb_6O_{24}$ ceramic obtained from the sintering at 1500°C for 4 hour has been examined by SEM and is shown in Figure 7, confirming the high density for the $Ba_8NiNb_6O_{24}$ pellet. The $Ba_8NiNb_6O_{24}$ pellet contains significant column-shaped grains with widths (~5-25 μm) and lengths (~60 μm), displaying anisotropic grain growth. Such anisotropic feature on the grain growth has been widely observed in other eight-layer hexagonal perovskite materials.[7,12,26-28]

Figure 8A displays complex impedance plot for the $Ba_8NiNb_6O_{24}$ pellet at 550°C, consisting of one large semicircular arc from the bulk response and a small tail from the grain-boundary response. The large semicircular arc can be modeled with a parallel *RC* circuit: the low-frequency intercept was estimated as *R* and the associated *C* calculated using $2\pi f_{max}RC=1$ equation (f_{max} is the frequency corresponding to the maximum imaginary impedance Z″) is ~4.9 pF/cm, consistent with the bulk response.[29] The Arrhenius plot of the bulk conductivities of $Ba_8NiNb_6O_{24}$ pellet is shown in Figure 8B, which shows a curvature around 650°C and increase of activation energy from 1.18 (9) eV (T<650°C) to 1.35(3) eV (T>650°C). Figure 9 shows the UV-Vis light absorption spectra of the $Ba_8NiNb_6O_{24}$ sample, which reveals a band gap of ~3.04 (2) eV for $Ba_8NiNb_6O_{24}$. Therefore, the increase of activation energy above 650°C could be ascribed to a conduction mechanism change from the impurity ionization at low temperature to the electron excitation over the intrinsic gap to conduction band at high temperature.[7,12]

TABLE 2 Bond lengths for $Ba_8NbNi_6O_{24}$

Bond	Lengths(Å)	Bond	Lengths(Å)
Ba_1–O_2(×3)	2.79(2)	Ba_5–O_4(×2)	3.05(1)
Ba_1–O_5(×6)	2.883(8)	Ba_5–O_4(×2)	2.77(2)
Ba_1–O_7(×3)	2.91(2)	Ba_5–O_6(×2)	2.99(2)
Ba_2–O_1(×3)	2.914(1)	Ba_5–O_7(×1)	2.90(2)
Ba_2–O_5(×3)	2.935(8)	Ba_5–O_8(×2)	2.91(2)
Ba_2–O_6(×3)	2.85(2)	Nb_1–O_4(×3)	2.13(2)
Ba_2–O_8(×3)	2.90(2)	Nb_1–O_8(×3)	2.18(2)
Ba_3–O_3(×1)	2.51(2)	Nb_2/Ni_2–O_4(×3)	2.08(2)
Ba_3–O_4(×2)	2.81(2)	Nb_2/Ni_2–O_6(×3)	2.11(2)
Ba_3–O_5(×2)	3.10(2)	Nb_3–O_3(×3)	1.86(2)
Ba_3–O_6(×2)	2.93(2)	Nb_3–O_7(×3)	2.24(2)
Ba_3–O_6(×2)	2.96(2)	Nb_4–O_1(×1)	1.94(2)
Ba_4–O_1(×1)	2.97(2)	Nb_4–O_7(×1)	1.90(2)
Ba_4–O_2(×2)	2.931(4)	Nb_4–O_5(×2)	2.07(2)
Ba_4–O_3(×1)	2.97(2)	Nb_4–O_6(×2)	1.99(2)
Ba_4–O_4(×2)	2.69(2)	Nb_5–O_1(×1)	2.20(2)
Ba_4–O_5(×2)	3.05(2)	Nb_5–O_2(×1)	2.03(2)
Ba_4–O_8(×2)	2.85(1)	Nb_5–O_5(×2)	2.06(2)
Ba_4–O_8(×2)	3.01(2)	Nb_5–O_8(×2)	1.87(2)
Ba_5–O_2(×1)	3.03(2)	Nb_6–O_2(×3)	2.12(2)
Ba_5–O_3(×2)	2.920(3)	Nb_6–O_3(×3)	2.18(2)

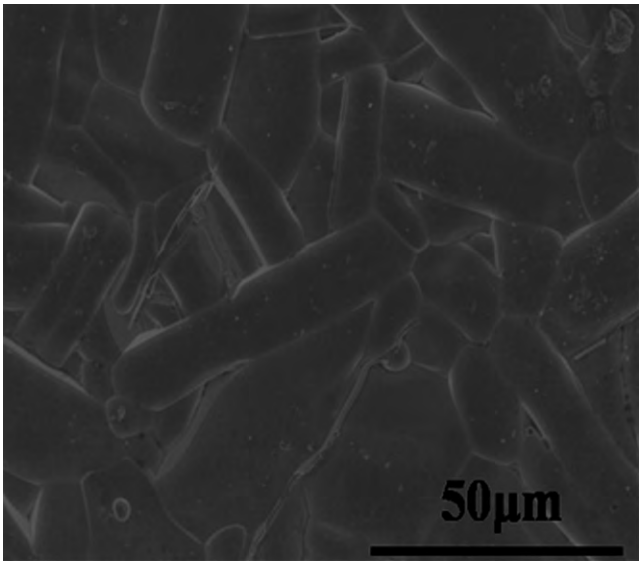

FIGURE 7 Typical scanning electron microscopy image of surface morphology of the $Ba_8NiNb_6O_{24}$ ceramic

The microwave dielectric measurement showed that the $Ba_8NiNb_6O_{24}$ pellet possesses dielectric constant $\varepsilon_r \sim 40$, modest quality factor $Qf \sim 32\,588$ GHz, and positive temperature coefficient of resonant frequency $\tau_f \sim 60$ ppm/°C. The as-made $Ba_8NiNb_6O_{24}$ pellets were further annealed at

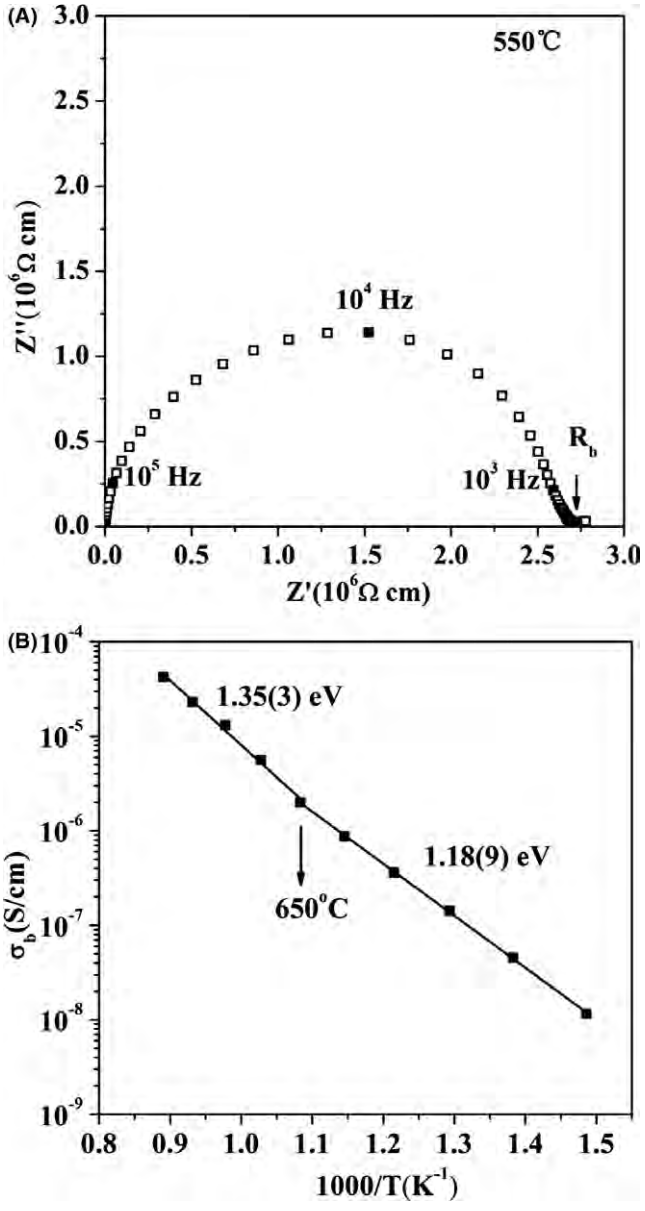

FIGURE 8 (A) Complex impedance plot recorded at 550°C and (B) Arrhenius plot of the bulk conductivity for $Ba_8NiNb_6O_{24}$ ceramic. Selected frequencies marked by the filled symbols in (A) are labeled. R_b denotes bulk resistivity

1400°C for 12-24 hour. Annealing at 1400°C for 12 hour improved the *Qf* value to 41 319 GHz. However, the prolonged annealing at 1400°C for 24 hour apparently deteriorated the *Qf* value down to 20 112 GHz. This could be ascribed to the partial decomposition, as revealed by the XRD data. The lower *Qf* values of $Ba_8NiNb_6O_{24}$ than Ba_8M-Ta_6O_{24}(*M*=Zn, Co, Ni)[11,12,15,16] may be linked with the more disordered FSO cations and vacancies in $Ba_8NiNb_6O_{24}$, given that the site/charge ordering effect on dielectric loss also takes place in the hexagonal perovskites (eg, $Ba_8ZnTa_6O_{24}$[30] and $Ba_8Ga_{4-x}Ta_{4+0.6x}O_{24}$[7]) in a way similar to the cubic perovskites. However, in general, the dielectric loss is highly sensitive to the ceramic processing, which also significantly

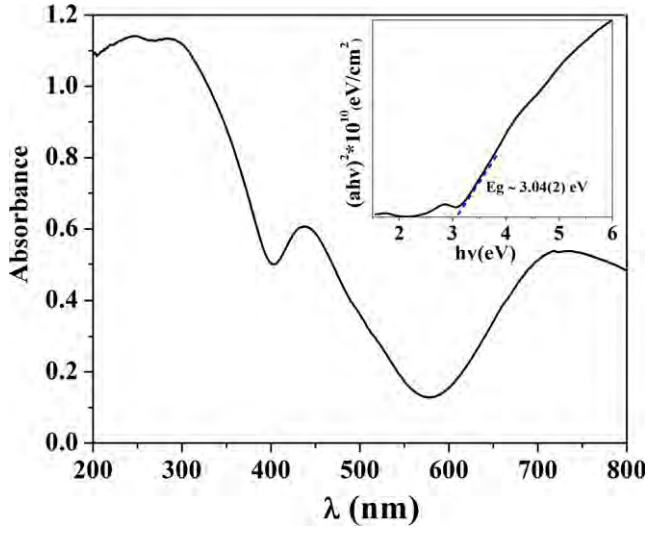

FIGURE 9 Ultraviolet and visible is light absorption spectrum of the $Ba_8NiNb_6O_{24}$. The inset shows plots of $(ahv)^2$ vs energy hv, for which the band gap is estimated as ~3.04 eV for $Ba_8NiNb_6O_{24}$ [Color figure can be viewed at wileyonlinelibrary.com]

impacts the other factors including porosity, minor secondary phase formation, and grain growth therefore affects the extrinsic dielectric loss.[1,7] The *Qf* value enhancement from the annealing at 1400°C for a short time of 12 hour is not well understood. This could be owing to the possible increase of the short-range cationic ordering inside the FSO dimers, which could be too small to be detected effectively by XRD. The dielectric loss response of $Ba_8NiNb_6O_{24}$ ceramics to the thermal annealing indicates that there could be still room for improving the *Qf* value of $Ba_8NiNb_6O_{24}$ via further optimizing the ceramic processing.

The dielectric permittivity of $Ba_8NiNb_6O_{24}$ is higher than those of $Ba_8MTa_6O_{24}$ (*M*=Co, Ni, Zn, ε_r ~ 27-29), which is in consistence with the more covalent character of the Nb^{5+}-O bond than Ta^{5+}-O.[4,15] The τ_f value for $Ba_8NiNb_6O_{24}$ is larger than $Ba_8MTa_6O_{24}$ (*M*=Co, Ni, Zn, τ_f ~ 29-44 ppm/°C), but lower than the twinned $Ba_4LiNb_3O_{12}$[31] and $Ba_8Ta_{4-0.8x}Ti_{3-x}O_{24}$ (τ_f ~ 65-76 ppm/°C),[32,33] which show permittivities (36-44) close to that for $Ba_8NiNb_6O_{24}$. Although the dielectric performance of $Ba_8NiNb_6O_{24}$ does not exceed the existing related materials, the results presented here contribute to understanding the interplay among chemical composition, structure, and properties of the existing shifted $Ba_8MNb_6O_{24}$ (*M*=Co, Zn) niobates and high-*Q* twinned $Ba_8MTa_6O_{24}$ (*M*=Co, Ni, Zn) tantalates.

4 | CONCLUSIONS

A new eight-layer hexagonal perovskite, $Ba_8NiNb_6O_{24}$, was synthesized and found to be isostructural with the twinned $Ba_8NiTa_6O_{24}$, but different from the shifted $Ba_8CoNb_6O_{24}$ and $Ba_8ZnNb_6O_{24}$ materials. $Ba_8NiNb_6O_{24}$ displays more disordered cation and vacancies over the FSO B-sites than the twinned tantalates $Ba_8MTa_6O_{24}$ (*M*=Zn, Ni, Co). Compared with $(Zn/Co)^{2+}$ and Nb^{5+} in the shifted $Ba_8ZnNb_6O_{24}$ (or $Ba_8CoNb_6O_{24}$), the smaller size difference between Ni^{2+} and Nb^{5+} plays an important role on the stabilization of $Ba_8NiNb_6O_{24}$ with a twinned structure. This smaller size difference could be also responsible for the reduced cation/vacancy ordering in $Ba_8NiNb_6O_{24}$. Finally, $Ba_8NiNb_6O_{24}$ shows higher permittivity ε_r ~ 40, but lower quality factor *Qf* ~ 41 319 GHz and larger temperature coefficient of resonant frequency τ_f ~ 60 ppm/°C than the twinned tantalates $Ba_8MTa_6O_{24}$. The lower *Qf* value of $Ba_8NiNb_6O_{24}$ is linked with the reduced short-range B-cationic ordering inside the FSO dimers compared with the high-*Q* $Ba_8MTa_6O_{24}$.

ACKNOWLEDGMENTS

The National Natural Science Foundation of China (No. 21361008, 21511130134, 21561008), NSFC-CNRS Bilateral TransLight Project (No. PICS07091), Guangxi Natural Science Foundation (No. 2015GXNSFFA139003), Guangxi Program for Hundred Talents for Returned Scholars and Guangxi Key Laboratory for Advanced Materials and New Preparation Technology (No. 12AA-11) are acknowledged for the financial support. Use of the Advanced Photon Source at Argonne National Laboratory was supported by the U.S. Department of Energy, Office of Science, Office of Basic Energy Sciences, under Contract No. DE-AC02-06CH11357. We also thank Prof. Wenfeng Zhu (Guilin University of Technology) for the assistance on the SEM experiment.

REFERENCES

1. Reaney IM, Iddles D. Microwave dielectric ceramics for resonators and filters in mobile phone networks. *J Am Ceram Soc*. 2006;89:2063–2072.
2. Davies PK, Borisevich A, Thirumal M. Communicating with wireless perovskites: cation order and zinc volatilization. *J Eur Ceram Soc*. 2003;23:2461–2466.
3. Hughes H, Iddles DM, Reaney IM. Niobate-based microwave dielectrics suitable for third generation mobile phone base stations. *Appl Phys Lett*. 2001;79:2952–2954.
4. Lufaso M. Crystal structure, modelling, and dielectric property relationships of 2:1 ordered $Ba_3MM'2O_9$ (M = Mg, Ni, Zn; M′ = Nb, Ta) perovskites. *Chem Mater*. 2004;16:2148–2156.
5. Wang J, Lu W, Lei W. Effects of Ba deficiency on ion ordering, grain growth, and microwave dielectric properties of $Ba_{1-x}Zn_{1/3}Nb_{2/3}O_3$ ceramics. *Jpn J Appl Phys*. 2012;51:041501–041505.
6. Cava RJ. Dielectric materials for applications in microwave communications. *J Mater Chem*. 2001;11:54–62.
7. Cao J, Kuang X, Allix M, et al. New -layer twinned hexagonal perovskite microwave dielectric ceramics $Ba_8Ga_{4-x}Ta_{4+0.6x}O_{24}$. *Chem Mater*. 2011;23:5058–5067.

8. Keith GM, Kirk CA, Sarma K, et al. Synthesis, crystal structure, and characterization of $Ba(Ti_{1/2}Mn_{1/2})O_3$: a high permittivity 12R-type hexagonal perovskite. *Chem Mater*. 2004;16:2007–2015.
9. Rawal R, McQueen AJ, Gillie LJ, et al. Influence of octahedral tilting on the microwave dielectric properties of $A_3LaNb_3O_{12}$ hexagonal perovskites (A=Ba, Sr). *Appl Phys Lett*. 2009;94:192904.
10. Vineis C, Davies PK, Negas T, Bell S. Microwave dielectric properties of hexagonal perovskites. *Mater Res Bull*. 1996;31:431–437.
11. Moussa SM, Claridge JB, Rosseinsky MJ, et al. $Ba_8ZnTa_6O_{24}$: a high-q microwave dielectric from a potentially diverse homologous series. *Appl Phys Lett*. 2003;82:4537–4539.
12. Thirumal M, Davies PK. $Ba_8ZnTa_6O_{24}$: a new high Q dielectric perovskite. *J Am Ceram Soc*. 2005;88:2126–2218.
13. Mallinson PM, Allix MMB, Claridge JB, et al. $Ba_8CoNb_6O_{24}$: a d^0 dielectric oxide host containing ordered d^7 cation layers 1.88 nm apart. *Angew Chem Int Ed*. 2005;44:7733–7736.
14. Trolliard G, Ténèze N, Boullay P, Mercurio D. TEM study of cation-deficient-perovskite related $A_nB_{n-1}O_{3n}$ compounds: the twin-shift option. *J Solid State Chem*. 2004;177:1188–1196.
15. Kan A, Ogawa H, Yokoi A, Ohsato H. Microwave dielectric properties of perovskite-like structured $Ba_8Ta_6(Ni_{1-x}M_x)O_{24}$ (M = Co, Cu, and Zn) solid solutions. *Jpn J Appl Phys*. 2006;45:7494–7498.
16. Kawaguchi S, Ogawa H, Kan A, Ishihara S. Microwave dielectric properties of $Ba_8Ta_6(Ni_{1-x}M_x)O_{24}$ (M = Zn and Mg) ceramics. *J Eur Ceram Soc*. 2006;26:2045–2049.
17. Lu F, Wang X, Pan Z, et al. Nanometer-scale separation of d^{10} Zn^{2+}-layers and twin-shift competition in $Ba_8ZnNb_6O_{24}$-based 8-layered hexagonal perovskites. *Dalton Trans*. 2015;44:13173–13185.
18. Coelho A. *TOPAS Academic V4*. Brisbane, Australia: Coelho Software; 2005.
19. Brown ID, Altermatt D. Bond-valence parameters obtained from a systematic analysis of the inorganic crystal-structure database. *Acta Crystallogr., Sect. B*. 1985;41:244–247.
20. Hakki BW, Coleman PD. A dielectric resonator method of measuring inductive capacities in the millimeter range. *IEEE Trans Microwave Theory Tech*. 1960;8:402–410.
21. Abakumov AM, Tendeloo GV, Scheglov AA, Shpanchenko RV, Antipov EV. The crystal structure of $Ba_8Ta_6NiO_{24}$: cation ordering in hexagonal perovskites. *J Solid State Chem*. 1996;125:102–107.
22. Evans R, Howard JAK, Evans JSO. α-$Bi_2Sn_2O_7$ – a 176 atom crystal structure from powder diffraction data. *J Mater Chem*. 2003;13:2098–2103.
23. Kuang X, Li Y, Ling CD, Withers RL, Evans IR. Oxide ion conductivity, phase transitions, and phase separation in fluorite-based $Bi_{38-x}Mo_{7+x}O_{78+1.5x}$. *Chem Mater*. 2010;20:4484–4494.
24. Kuang X, Li MR, Chong SY, et al. Interstitial oxide ion order and conductivity in $La_{1.64}Ca_{0.36}Ga_3O_{7.32}$ melilite. *Angew Chem In Ed*. 2010;49:2362–2366.
25. Davies PK, Tong J, Negas T. Effect of ordering-induced domain boundaries on low-loss $Ba(Zn_{1/3}Ta_{2/3})O_3$-$BaZrO_3$ perovaskite microwave dielectrics. *J Am Ceram Soc*. 1997;80:1727–1740.
26. Yu X, Chai S, Kuang X, et al. Conductivity, dielectric loss, and electrical heterogeneous microstructure of eight-layer twinned hexagonal perovskite ceramics $Ba_8CuTa_6O_{24-\delta}$. *J Am Ceram Soc*. 2013;96:2510–2514.
27. Thirumal M, Davies PK. Tunable high Q perovskite dielectrics in the BaO–NiO–Ta_2O_5 system. *J Mater Sci*. 2011;46:4715–4718.
28. Rawal R, Feteira A, Flores AA, et al. Dielectric properties of the "twinned" 8H-hexagonal perovskite $Ba_8Nb_4Ti_3O_{24}$. *J Am Ceram Soc*. 2006;89:336–339.
29. Irvine JTS, Sinclair DC, West AR. Electroceramics: characterization by impedance spectroscopy. *Adv Mater*. 1990;2:132–138.
30. Mallinson P, Claridge JB, Iddles D, et al. New 10-layer hexagonal perovskites: relationship between cation and vacancy ordering and microwave dielectric loss. *Chem Mater*. 2007;38:6227–6238.
31. Fang L, Li CC, Peng XY, Hu CZ, Wu BL, Zhou HF. $Ba_4LiNb_{3-x}Ta_xO_{12}$ (x=0-3): a series of high-Q microwave dielectrics from the twinned 8H hexagonal perovskites. *J Am Ceram Soc*. 2010;93:1229–1231.
32. Baranov AN, Oh YJ. Microwave frequency dielectric properties of hexagonal perovskites in the $Ba_5Ta_4O_{15}$–$BaTiO_3$ system. *J Eur Ceram Soc*. 2005;25:3451–3457.
33. Yokoi A, Ogawa H, Kan A. Microwave dielectric ceramics for resonators and filters in mobile phone networks. *J Eur Ceram Soc*. 2006;26:2069–2074.

How to cite this article: Tao F, Wang X, Gong M, et al. New eight-layer twinned hexagonal perovskite microwave dielectric ceramic $Ba_8NiNb_6O_{24}$. *J Am Ceram Soc*. 2017;100:1212–1220.